Journal of Materials Chemistry B

ROYAL SOCIETY OF CHEMISTRY

PAPER

View Article Online
View Journal | View Issue

Cite this: J. Mater. Chem. B, 2023, 11, 11344

Development of bioactive and ultrasound-responsive microdroplets for preventing ovariectomy (OVX)-induced osteoporosis†

Yi Zhang,‡[ac] Yi Dang,‡[b] Maodi Huang,[b] Yaping Ma,[b] Dingmei Zhang[b] and Xin Wang *[bd]

Received 31st July 2023,
Accepted 7th November 2023

DOI: 10.1039/d3tb01726e

rsc.li/materials-b

As a common bone disease in the elderly population, osteoporosis-related bone loss and bone structure deterioration represent a major public health problem. Therapeutic strategies targeting excessive osteoclast formation are frequently used for osteoporosis treatment; however, potential side effects have been recorded. Here, we have developed a novel therapeutic strategy using microdroplets (MDs) encapsulated with NFATc1-siRNA and investigated the role of bioactive MDs-NFATc1 biocompatibility in RAW 264.7 macrophages and human mesenchymal stem cells (hBMSCs), respectively. Its role in regulating osteoclast differentiation and formation was also investigated *in vitro*. We first fabricated MDs with spherical morphology along with a well-defined core–shell structure. The ultrasound-responsive study demonstrated time-dependent responsive structural changes following ultrasound stimulation. The internalization study into unstimulated macrophages, inflammatory macrophages, and hBMSCs indicated good delivery efficiency. Furthermore, the results from the MTT assay, the live/dead assay, and the cellular morphological analysis further indicated good biocompatibility of our bioactive MDs-NFATc1. Following MDs-NFATc1 treatment, the number of osteoclasts was greatly reduced, indicating their inhibitory effect on osteoclastogenesis and osteoclast formation. Subsequently, osteoporotic rats that underwent ovariectomy (OVX) were used for the *in vivo* studies. The rats treated with MDs-NFATc1 exhibited significant resistance to bone loss induced by OVX. In conclusion, our results demonstrate that MDs-NFATc1 could become an important regulator in osteoclast differentiation and functions, thus having potential applications in osteoclast-related bone diseases.

Introduction

Osteoporosis is a bone disease characterized by deterioration of bone tissue microstructure and loss of bone mass, which increases bone fragility and susceptibility to fracture. It is a major public health problem with the aging of the world population.[1,2] About 10 million Americans over the age of 50 have osteoporosis, and 34 million are at risk of osteoporosis in the US.[3] Osteoporotic fractures are extremely common in the US, with about 1.5 million people suffering from brittle fractures each year. A similar burden of disease has been observed in the UK, where epidemiological studies assume that one in two women and one in five men over the age of 50 may suffer an osteoporotic fracture in their lifetime.[4] The economic burden of fractures associated with osteoporosis is substantial, with an annual cost of approximately $17.9 billion in the USA and £4 billion in the UK each year.[5] Additionally, it is projected that osteoporosis-related fractures will impose an annual cost of approximately $50 billion in the US healthcare system by 2040.[1] Worldwide, the economic burden of osteoporosis and osteoporotic fracture is similar to that in the United States.[6]

Bone undergoes a constant process of resorption by osteoclasts and renewal orchestrated by osteoblasts. Maintaining a delicate equilibrium between osteoclast-driven bone resorption and osteoblast-mediated bone formation, and regulating these processes, is vital for the maintenance of bone density and homeostasis.[7] Osteoporosis occurs due to an imbalance in the remodeling process.[8] Various factors, including post menopause, aging, medications, endocrine disorders, *et al.*, can

[a] Department of Hygiene Toxicology, Zunyi Medical University, Zunyi, 563000 Guizhou, China
[b] Department of Orthopaedic Surgery, Affiliated Hospital of Zunyi Medical University, Zunyi, 563003 Guizhou, China. E-mail: xin.wang@zmu.edu.cn; Fax: +86-851-2860 8903; Tel: +86 136 3928 8558
[c] Key Laboratory of Maternal & Child Health and Exposure Science of Guizhou Higher Education Institutes, Zunyi Medical University, Zunyi, 563000 Guizhou, China
[d] Guizhou Provincial Key Laboratory of Medicinal Biotechnology in Colleges and Universities, Zunyi Medical University, Zunyi, 563000 Guizhou, China

† Electronic supplementary information (ESI) available. See DOI: https://doi.org/10.1039/d3tb01726e

‡ Yi Zhang and Yi Dang contributed equally to this work and are considered co-first authors.

contribute to the imbalance in the remodeling process, which in turn, lead to osteoporosis.[8]

Bisphosphonates are the most frequently prescribed medications for osteoporosis treatment. However, long-term usage can result in unsatisfactory clinical outcomes and complications, including atypical fractures and decreased bone strength, according to a review study by the American Society for Bone and Mineral Research (ASBMR).[9] Additionally, a high dose of bisphosphonates can lead to more severe gastrointestinal issues. Parathyroid hormone (PTH) therapy is currently employed as an anabolic approach to stimulate bone formation. However, the use of PTH therapy has been associated with several side effects.[10] Hence, there is an urgent need for innovative therapies aimed at addressing the imbalances in bone remodeling.

Microdroplets (MDs) are small carriers, which are currently used as effective drug/gene delivery systems because they can deliver drugs/genes selectively to target sites.[11] MDs are an enticing prospect for the distribution of therapeutics and have demonstrated improved cancer aggregation and retention.[12,13] Furthermore, the exceptional stability of MDs increases their use in various biomedical applications.[14,15] Moreover, they are often used either to mediate or cause therapeutic effects.[16] Recently, they have also been employed for the transmission of medications, chromosomes, and gas.[17,18] Ultrasound is one of the most commonly used methods in the diagnosis and therapy of diseases due to its safety, deep penetration into tissues, and non-invasive nature.[19] Ultrasound demonstrates numerous advantages in drug/gene co-delivery systems, specifically in achieving site-specific delivery and spatial release control of drugs/genes, thereby garnering growing attention.[19,20] Ultrasound-based gene/drug release systems have found applications in treating various conditions such as ischemia-reperfusion liver injury,[21] thrombolysis,[22] Parkinson's disease,[23] and so on. Therefore, it is the most promising targeted therapy method at present and is expected to be widely used in the therapy of multiple diseases.

Binding of receptor activator of nuclear factor kappa-B (RANK) and its ligand RANKL is essential for osteoclast development and activation.[24] As a type I transmembrane protein, RANK transduces intracellular signals by recruiting different adaptor proteins, including TNFR-associated factor 6 (TRAF6), *etc.*[25] Additionally, the expression and translocation of nuclear factor of activated T cells cytoplasmic 1 (NFATc1) serve as a master regulator for osteoclast differentiation[26] and the expression of osteoclastic genes.[27] Therefore, in this study, we intend to generate a novel osteoclastogenesis-targeted therapeutic strategy to regulate osteoclast differentiation and formation. In the end, this study may provide a novel therapeutic option in the prevention and treatment of bone remodeling imbalance or other similar mechanism-mediated bone diseases.

Materials and methods

Cell culture

Human bone marrow-derived mesenchymal stromal cells (hBMSCs, ATCC® PCS-500-012™) were used for this study. Cells were cultured in Dulbecco's Modified Eagle's Medium (DMEM; Life Technologies Pty Ltd, China) supplemented with 10% fetal bovine serum (FBS; Biological Industries, LTD, Beit Haemek, Israel), and 1% (v/v) penicillin/streptomycin (Solarbio, Beijing, China) in an atmosphere of 5% CO_2 at 37 °C. The murine-derived macrophage cell line, RAW264.7 cells (ATCC® TIB-71™), was maintained in DMEM supplemented with 10% heat-inactivated FBS and 1% (v/v) penicillin/streptomycin in a humidified incubator containing 5% CO_2 at 37 °C.

Fabrication and characterization of MDs

MDs, scramble siRNA-loaded MDs (MDs-scramble), and NFATc1 siRNA-loaded MDs (MDs-NFATc1) were fabricated accordingly. Briefly, a mixture of 50 nM NFATc1 siRNA (sc-29412, Santa Cruz Biotechnology), 300 μL of perfluorocarbon, 4 mL of PBS, and 40 mg of bovine serum albumin (BSA, Sigma Aldrich, China) were sonicated for MD fabrication. The resulting emulsion was ultracentrifuged (Beckman Coulter, Optima XPN-100, USA) at 14 000 rpm for 30 min. Fluorescence-labeled MDs-NFATc1 was fabricated using fluorescein isothiocyanate (FITC)-labelled BSA (Sigma, China) with the same formulation mentioned above. Fluorescence-labeled MDs-NFATc1 was used for MD characterization using a confocal laser scanning microscope (Leica DM IRB; Leica, Wetzlar, Germany). Briefly, 5 mg of MDs-NFATc1 were diluted in 1 mL PBS, stimulated with an ultrasound probe with an acoustic frequency of 1 MHz using a portable home use ultrasound pain therapy device for 15 min (MYCHWAY, China). The activated MDs-NFATc1 was then observed using a confocal laser scanning microscope with a ×40 objective (Leica DM IRB; Leica, Wetzlar, Germany). MDs-NFATc1 growth and rupture were observed using an inverted light microscope (Leica, Wetzlar, Germany). Briefly, the samples were exposed to an ultrasound probe with an acoustic frequency of 1 MHz using a portable home use ultrasound pain therapy device for 15 min (MYCHWAY, China). Images were captured using an inverted light microscope (Leica, Wetzlar, Germany) at indicated time points.

Internalization of MDs into cells

MD internalization into cells was evaluated by confocal laser scanning microscopy. Briefly, cells were treated with FITC-labeled MDs for indicated time periods. After rinsing with PBS, cells were fixed with 4% paraformaldehyde and stained with Alexa Fluor 594-labeled phalloidin (Thermo Fisher Scientific, China). Images of the stained samples were examined using a confocal laser scanning microscope with a ×40 objective (Leica DM IRB; Leica, Wetzlar, Germany). To induce inflammatory macrophage polarization, macrophages were stimulated with 1000 ng mL^{-1} of lipopolysaccharide (LPS, *Escherichia coli* 0111: B4, Sigma, China), as established in our previous study.[28]

MTT assay

MTT cell proliferation assay was used to evaluate cell viability according to the manufacturer's instructions. Briefly, 20 μL of 5 mg mL^{-1} 3-(4,5-dimethylthiazol-2-yl)-2,5-diphenyl tetrazolium bromide (MTT, M2128, Sigma, China) was added to the cells and

incubated for an additional 4 h at 37 °C. After carefully removing the supernatant, purple MTT formazan crystals were dissolved in 100 μL dimethyl sulfoxide (DMSO). The absorbance values of each sample were measured at 570 nm using an enzyme-linked immunosorbent assay reader.

Cell morphological analysis

Cell morphology was examined by confocal laser scanning microscopy *via* phalloidin/DAPI staining. Briefly, the cells were rinsed with PBS, fixed with 4% paraformaldehyde, permeabilized, and stained with Alexa Fluor 594-labeled phalloidin (Thermo Fisher Scientific, China) for 1 h. Samples were then mounted with ProLong™ Gold Antifade Mountant with DAPI (P36935, Thermo Fisher Scientific, China) and the images of the stained samples were examined using a confocal laser scanning microscope with a ×10 objective (Leica DM IRB; Leica, Wetzlar, Germany).

Live and dead assay

Live/dead staining was performed according to the manufacturer's instructions (C2015M, Beyotime, China). Briefly, cells were stained with Calcein AM/PI staining solution and incubated at 37 °C for 30 min. After washing with PBS, samples were viewed using an inverted fluorescence microscope with a ×10 objective (Leica, Wetzlar, Germany).

Tartrate-resistant acid phosphatase (TRAP) staining

TRAP staining was used to assess the effects of different formulations of MDs on the differentiation of osteoclast precursors. Briefly, human osteoclast precursors were cultured with different formulations of MDs in an osteoclast precursor growth medium supplemented with 1% (v/v) penicillin/streptomycin, 10% FBS, 2 mM L-glutamine, M-CSF and RANKL. TRAP staining was performed as previously described.[29] Briefly, cells were washed with PBS and fixed with 4% paraformaldehyde for 10 min. After staining, purple-to-red multinucleated TRAP-positive cells containing three or more nuclei were considered as osteoclast cells.

Actin ring staining

Cells were rinsed with PBS, fixed with 4% paraformaldehyde, permeabilized, and stained with Alexa Fluor 594-labeled phalloidin (Thermo Fisher Scientific, China) for 1 h. Samples were then mounted with ProLong™ Gold Antifade Mountant with DAPI (P36935, Thermo Fisher Scientific, China). The fluorescence images were examined using a confocal laser scanning microscope with a ×20 objective (Leica DM IRB; Leica, Wetzlar, Germany).

Bone resorption pit

Human osteoclast precursors were seeded onto bone discs and cultured in the presence of various formulations of MDs in the osteoclast precursor growth medium, as described earlier. The bone discs were then fixed using 4% paraformaldehyde and subsequently stained with DAPI. To investigate the formation of resorption pits, a confocal laser scanning microscope was employed to visualize the bone surface using a ×10 objective (Leica DM IRB; Leica, Wetzlar, Germany).

Animal study

Female Sprague-Dawley (SD, 8 weeks old) rats that underwent ovariectomy (OVX) or sham-operated (sham) were used for this study. All animal experiments were in accord with institutional animal use and care regulations approved by the Zunyi Medical University Committee (ZMU21-2203-009). The rats were divided into four groups (1. Sham; 2. OVX; 3. OVX + MDs-scramble (20 mg kg^{-1} in saline); and 4. OVX + MDs-NFATc1 (20 mg kg^{-1} in saline)), with each group consisting of five animals. Intraperitoneal (I.P.) injections were administered twice a week, on day 1 and day 4. The rats were euthanized at 10 weeks, and their femurs were harvested for subsequent histological analysis.

Histological assessment

To perform haematoxylin and eosin (H&E) staining, the bones were first carefully extracted and cleaned to remove any surrounding soft tissue. Subsequently, they were fixed in 10% neutral buffered formalin. Decalcification was then carried out using a 10% ethylenediaminetetraacetic acid (EDTA, pH 7.4) solution. After decalcification, the samples were embedded in paraffin wax and were cut into sections with a thickness of 5 μm using a microtome. Subsequently, the sections underwent sequential staining using a Hematoxylin–Eosin (H&E) Staining Kit (Beyotime, Shanghai, China). To analyze the presence and activity of osteoclasts within the samples, TRAP staining was performed using the methods describe above. Following the washing step with distilled water, the cell nuclei were counterstained with hematoxylin solution for 5 min. Images of the stained sections were obtained using an inverted microscope with a ×10 objective (Leica, Wetzlar, Germany).

Enzyme-linked immunosorbent assay (ELISA) analysis

Serum levels of C-terminal telopeptides of type I collagen (CTX-1) were measured using ELISA kits (Bio-Techne, China) according to the manufacturer's instructions. The concentrations of CTX-1 were quantified based on the standard curve.

Statistical analysis

All data were expressed as mean ± standard deviations (SD). Statistical analysis was performed using GraphPad Prism 7 (Version 7.02) for Windows (GraphPad Software Inc., USA). Statistical differences between groups were determined with one-way analysis of variance (ANOVA). A value of $p < 0.05$ was considered statistically significant.

Results and discussion

Synthesis and characterization of bioactive MDs

The structure of MDs-NFATc1 is shown in Fig. 1(A). Fluorescence-labeled MDs were first fabricated using FITC-conjugated BSA. As shown in Fig. 1(A), confocal laser scanning microscopy images demonstrated spherical MDs with a FITC-

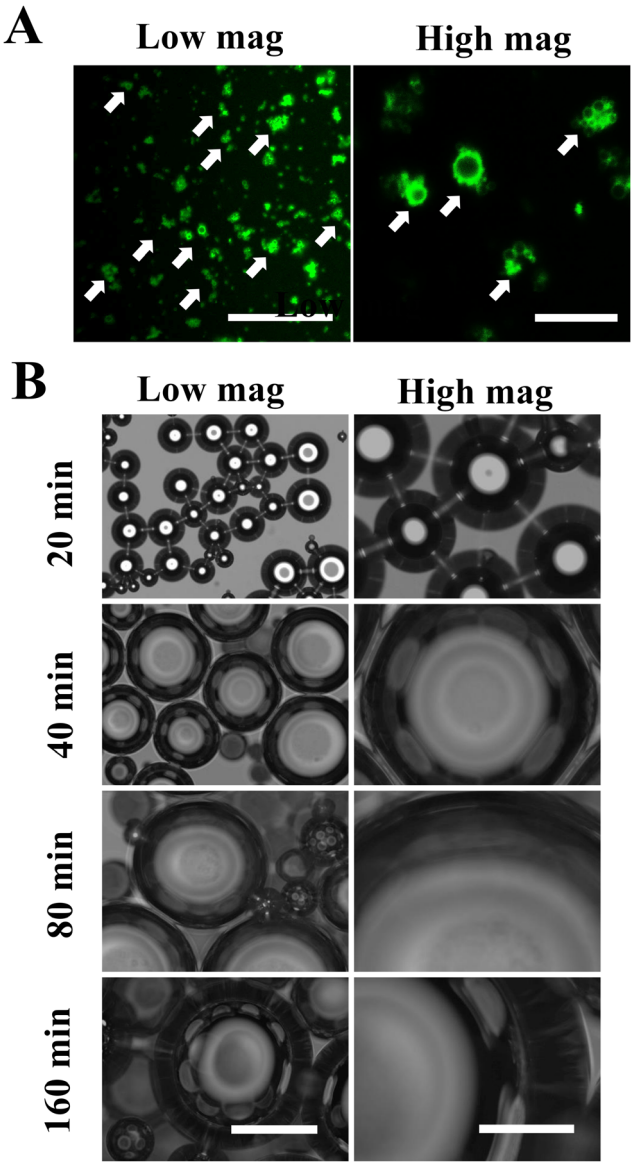

Fig. 1 Fabrication of bioactive-MDs-NFATc1. (A) Representative confocal laser scanning microscopy images showing MDs after encapsulation with NFATc1 siRNA. Scale bar = 50 μm (left), scale bar = 10 μm (right). (B) Representative micrographs showing MDs-NFATc1 growth after ultrasound stimulation. Scale bar = 500 μm (left), scale bar = 150 μm (right).

labeled (green color) shell structure. The time-dependent responsiveness of fluorescent-labeled MDs was next investigated using confocal laser scanning microscopy. As shown in Fig. 1(B), the morphology of MDs in response to ultrasound stimulation was observed *in vitro* and showed gradual size expansion at 20 min, 40 min, 80 min, and 160 min.

Confocal microscopy imaging of internalization of MDs into macrophages

Although siRNA therapy holds significant therapeutic potential, several barriers limit their clinical application.[30] Naked and unmodified siRNA is unable to cross the anionic cell plasma membrane and reach its target, which is one of the many limitations of siRNA-based therapy.[31,32] Additionally, the stability of unmodified or unprotected siRNA is not satisfactory, as they are extremely sensitive to endogenous RNases- and phosphatases-mediated degradation.[33] Therefore, after successful fabrication of MDs-NFATc1, we sought to validate the efficiency of cellular uptake of MDs-NFATc1 into mammalian cells. Macrophages are crucial cells for both the innate and adaptive immune systems and play an important role in tissue homeostasis, inflammation, and wound healing.[34] As precursors of osteoclast, monocyte/macrophage precursor cells adhere to the bone surface and develop into osteoclasts in the bone remodeling process.[35]

Next, the cellular internalization and localization of MDs were first observed using confocal laser scanning microscopy in unstimulated macrophages. As shown in Fig. 2(A), when the cells were treated with ultrasound-stimulated bioactive MDs, the MDs were able to access the cytoplasm and clustered around the peri-nuclei areas, indicating successful internalization of MDs into RAW264.7 macrophages. In addition, intense intracellular accumulation of green fluorescence was noted at 6 h post-stimulation when compared to their non-treated counterparts (Fig. 2(B)), indicating that satisfactory delivery efficiency of siRNA has been achieved.

Confocal microscopy imaging of internalization of MDs into inflammatory macrophages

In general, depending on their activation and polarization states, macrophages can be categorized as classically activated macrophages (M1 state) and alternatively activated macrophages (M2 state).[36] In recent years, it has become increasingly evident that the bone and immune system are functionally interconnected, as chronic inflammatory conditions and age-related disorders have a significant impact on bone homeostasis and turnover.[37] Under chronic and systemic inflammation, macrophages possess the capability to fuse and develop into multinucleated cells, potentially playing a direct role in osteoporosis development.[38] In addition, the secretion of various pro-inflammatory cytokines by these inflammatory macrophages may either directly or indirectly stimulate osteoclast differentiation and subsequent bone resorption.[39,40] Therefore, in order to further validate the successful internalization of MDs into inflammatory macrophages, we chose to induce macrophages into inflammatory phenotypes and examined the cellular uptake of MDs in these inflammatory macrophages using confocal laser scanning microscopy. Compared to the results obtained from the non-stimulated macrophages, our results indicated increased cellular uptake by inflammatory macrophages with peri-nuclear subcellular localization (Fig. 3(A)). Green fluorescence was noted within 1 h inside inflammatory macrophages, and the accumulation and intensity significantly increased following the incubation time. M1 macrophages are characterized with a higher level of phagocytic activity when compared with M0 macrophages,[41] along with high production of pro-inflammatory cytokine and nitric oxide (NO).[42] Therefore, the observed higher FITC-MDs uptake ability may contribute to M1 macrophage's phagocytic ability. As shown in Fig. 3(B), inflammatory macrophages without FITC-MDs-NFATc1 treatment

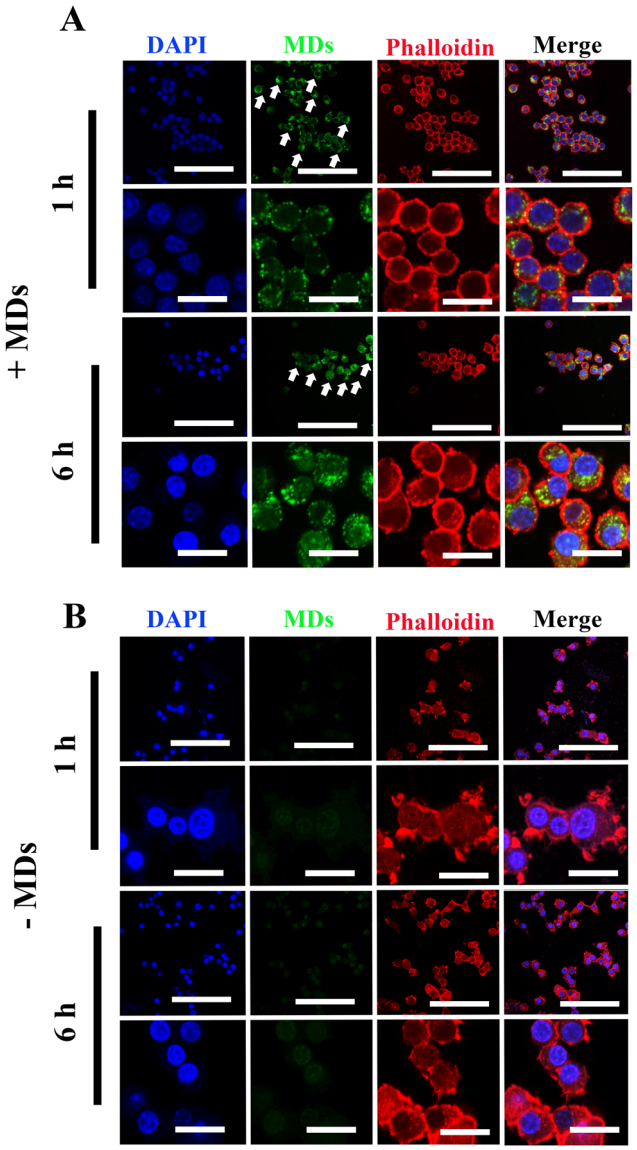

Fig. 2 Internalization of MDs into RAW264.7 macrophages. (A) Representative confocal laser scanning microscopy images showing the delivery of FITC-MDs-NFATc1 into RAW264.7 cells at indicated time points (1 h and 6 h). RAW264.7 macrophages were treated with FITC-MDs-NFATc1 as described in the Material and methods section. Cell cytoskeletons are shown in red color, while the blue channel indicates the nuclear staining. Scale bar = 100 μm (low magnification), scale bar = 20 μm (high magnification). The FITC-MDs-NFATc1 is denoted by the white arrow. (B) Cells without FITC-MDs-NFATc1 treatment at 1 h and 6 h post-treatment. Scale bar = 100 μm (low magnification), scale bar = 20 μm (high magnification).

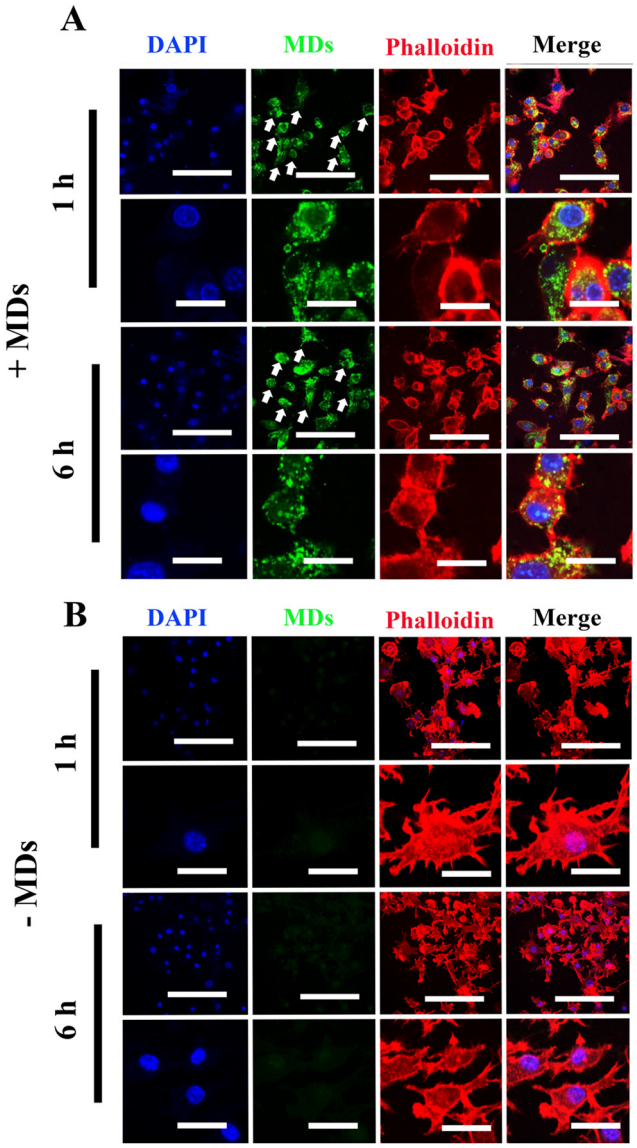

Fig. 3 Internalization of MDs into inflammatory macrophages. (A) Representative confocal laser scanning microscopy images indicating FITC-MDs-NFATc1 internalization into inflammatory macrophages. Inflammatory macrophages were treated with FITC-MDs-NFATc1 for 1 h and 6 h, respectively. Cell cytoskeletons and nuclei are shown in red and blue color, respectively. Scale bar = 100 μm (low magnification), scale bar = 20 μm (high magnification). The FITC-MDs-NFATc1 is denoted by the white arrow. (B) Cells without FITC-MDs-NFATc1 treatment were used as control. Scale bar = 100 μm (low magnification), scale bar = 20 μm (high magnification).

showed no intracellular accumulation of green fluorescence. While not the primary focus of this study, it is worth noting that we also observed the uptake of FITC-MDs in hBMSCs, as shown in Fig. S1 in the ESI.†

Biocompatibility of different formulations of MDs in macrophages

Transfection reagent-based siRNA delivery is the most widely used method for siRNA delivery into mammalian cells. However, many transfection reagents on the market exhibit considerable cytotoxicity,[43] especially when cellular functional studies need to be investigated subsequently.[44] Therefore, in this study, we evaluated macrophage viability following incubation with MDs-NFATc1 by conducting MTT assays at 1 day and 3 days time points.[28] The MTT assay is one of the most frequently used methods to analyze cell proliferation, viability, and cytotoxicity.[45] As shown in Fig. 4(A) and (B), the OD values of metabolically active macrophages cultured with different formulations of MDs showed similar OD

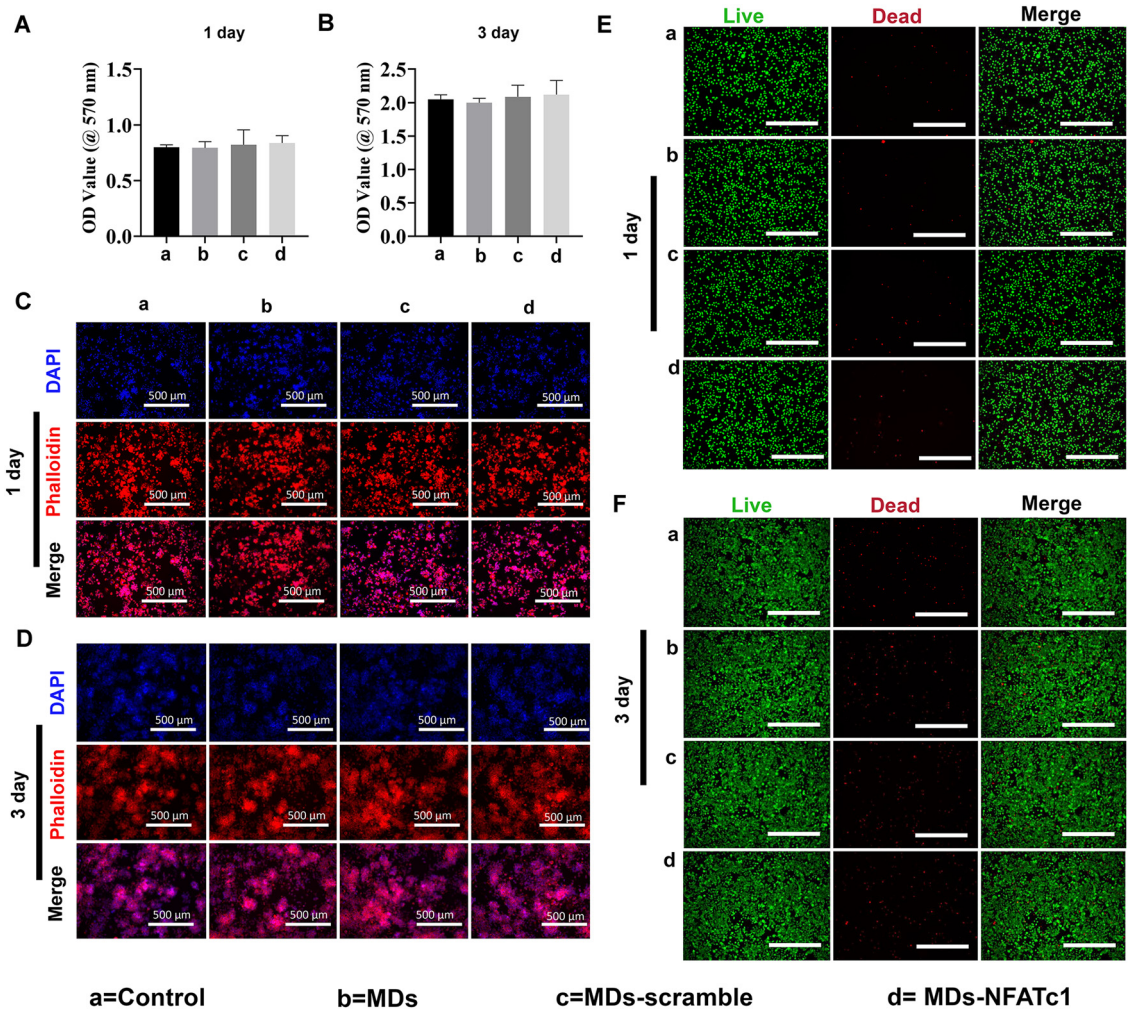

Fig. 4 Biocompatibility and morphology of macrophages following MD treatment. (A) Viability of RAW264.7 cells under MD exposure as evaluated by MTT assay on day 1. (B) Cell viability in RAW264.7 cells treated with or without MDs determined by MTT assay on day 3. (C) Representative confocal laser microscopy images of RAW264.7 cells after DAPI/phalloidin staining at day 1. Actin filaments were stained with phalloidin (red), while nuclei were stained with DAPI (blue). Scale bar = 500 μm. (D) Confocal analysis of RAW264.7 cells treated with or without MDs following DAPI/phalloidin staining on day 3. Scale bar = 500 μm. (E) Representative confocal laser microscopy images of RAW264.7 macrophages treated with or without MDs on day 1. Viable cells are indicated as green color (calcein-AM), while dead cells are labeled as red fluorescence (PI). Scale bar = 500 μm. (F) Representative confocal laser microscopy images of RAW264.7 macrophages treated with or without MDs after live/dead staining on day 3. Scale bar = 500 μm. Group a = control, group b = MDs, group c = MDs-scramble siRNA, and group d = MDs-NFATc1.

values compared to the non-treated control on day 1. Additionally, the OD values increased dramatically at day 3 compared to day 1 in MDs-NFATc1-treated cells, suggesting that the bioactive MDs-NFATc1 showed no signs of cytotoxicity on macrophages. Next, we investigated the biocompatibility of different formulations of MDs in macrophages using phalloidin/DAPI staining at indicated time-points. Fig. 4(C) and (D) show the fluorescence images of cytoskeleton and nuclei staining of macrophages after culturing with different formulations of materials at 1 day. The cells retain extensive cytoskeleton staining after 1 day treatment. At day 3, the macrophage numbers achieved a cell density comparable with non-treated macrophages, indicating good compatibility of bioactive MDs-NFATc1 in macrophages.

Previous study reported that the liposome–nanobubble conjugate with paclitaxel showed pro-apoptotic and cytotoxic effects on different cancer cells.[46] To further observe the cytotoxicity of macrophages treated with different formulations of MDs, the cells were stained with Calcein AM and propidium iodide (PI), which specifically stained live and dead cells, respectively.[47] As shown in Fig. 4(E) and (F), the macrophages treated with different formulations of MDs displayed intense green fluorescence, indicating that most of the cells were alive on day 1. On day 3, the population of live macrophages was greatly increased, as indicated by intense green fluorescence staining in all groups. These results suggested that bioactive MDs-NFATc1 showed good biocompatibility in macrophages.

Biocompatibility of bioactive MDs-NFATc1 in hBMSCs

Due to their high differentiation capacity, MSCs can differentiate into multiple lineages, including bone cells, chondrocytes,

adipose cells, *etc.*[48] Therefore, MSCs are one of the most frequently used stem cells for cell therapies and tissue engineering[49] due to their excellent self-renewal and differentiation capacity.[50] Bone marrow, adipose tissue, umbilical cord blood, placenta, *etc.* are the main donor sources of MSCs.[51] Additionally, previous studies have indicated that MSCs can secrete various chemokines, cytokines, and growth factors, including vascular endothelial growth factor, transforming growth factor-beta, stromal-derived

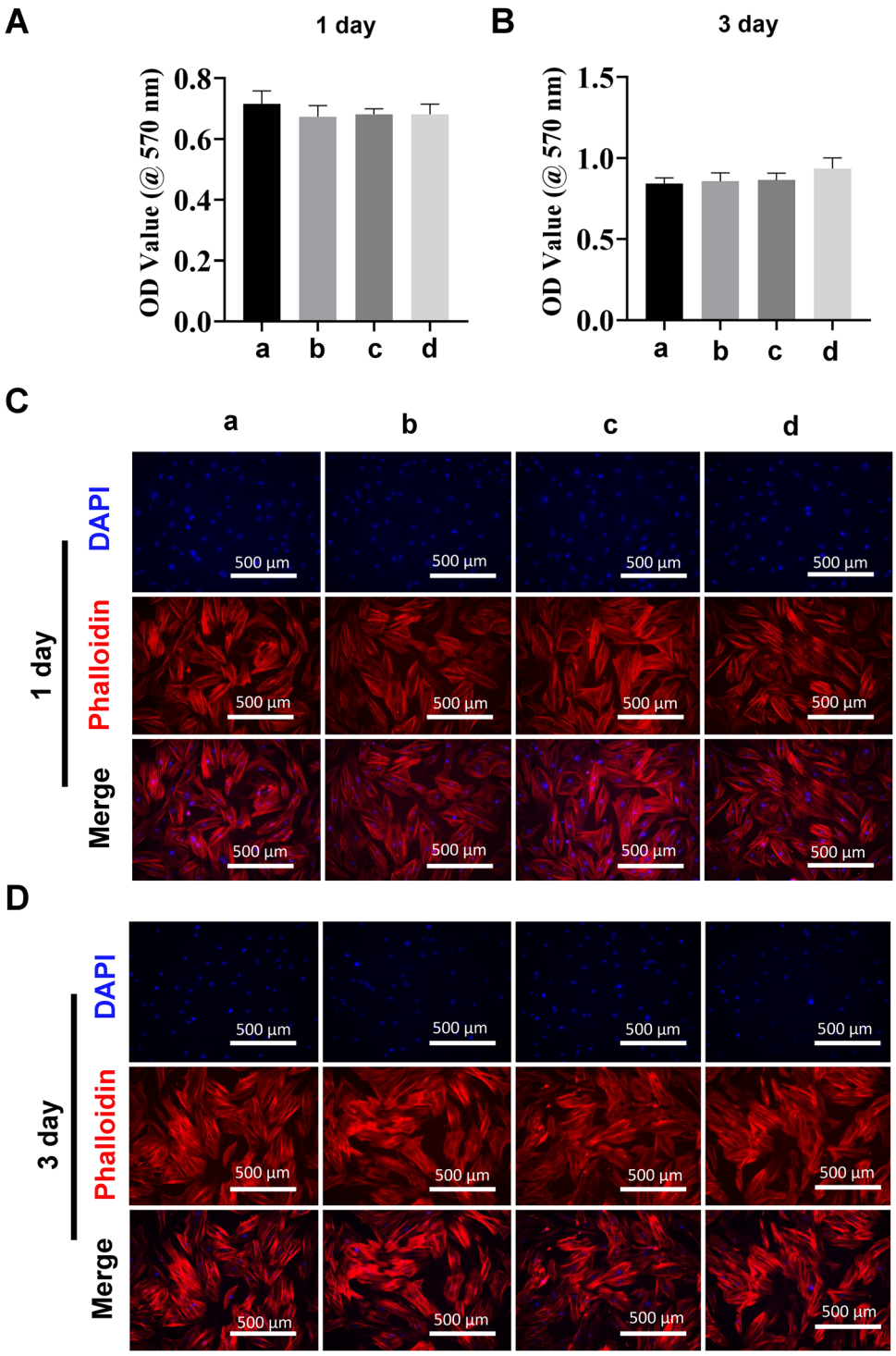

Fig. 5 Biocompatibility, viability, and morphology of hBMSCs. (A) MTT viability assay of hBMSCs at day 1 cultured with MDs. (B) Cell proliferation was evaluated by MTT viability assay at day 3. (C) Representative confocal laser scanning microscopy images showing hBMSC morphology using DAPI/phalloidin staining at day 1. The blue channel indicates nuclear staining, while the red channel demonstrates actin filament staining. (D) Representative images showing F-actin cytoskeletal morphology in hBMSCs on day 3. The blue channel indicates nuclei staining by DAPI, while the red channel represents phalloidin staining. Group a = control, group b = MDs, group c = MDs-scramble, and group d = MDs-NFATc1. All scale bar = 500 μm.

factor-1, monocyte chemotactic protein-1, platelet-derived growth factor polypeptide, *etc.*[52] Therefore, we next analyzed the biocompatibility of different formulations of MDs on hBMSCs at different timepoints using MTT assay, which showed no significant differences (Fig. 5(A) and (B)). We next evaluated the effects of different MDs on the morphological changes of hBMSCs. Fig. 5(C) and (D) show the confocal laser scanning microscopy imaging of fluorescently stained hBMSCs after treatment with or without different formulations of MDs at day 1 and day 3. Phalloidin and DAPI staining demonstrated similar growth patterns among different groups. MSCs showed intense cytoskeleton staining with no significant morphological changes among different groups.

MDs-NFATc1 inhibits RANKL-induced osteoclast formation *in vitro*

To investigate the effect of bioactive MDs-NFATc1 on osteoclast formation, human osteoclast precursors were incubated with different formations of MDs in the presence of RANKL and M-CSF for 7 days, respectively. Bone homeostasis is a dynamic balance maintained by the regulatory actions of the bone resorbing osteoclast and the bone forming osteoblast.[53] Osteoclasts are multinuclear giant cells of hemopoietic origin that resorb bone, containing between 3 and 10 nuclei,[54] and are important in maintaining healthy bone turnovers.[55] However, elevated expression of osteoclasts and bone resorption are frequently reported in different inflammatory bone diseases, such as osteoarthritis, osteoporosis, rheumatoid arthritis, osteomyelitis, *etc.*[56] The interaction between RANKL and RANK receptor on the surface of osteoclast precursors plays a key role in osteoclast differentiation and maturation.[57] Alterations in RANK/RANKL signaling were specifically targeted to control osteoclast formation and bone resorption.[58] For instance, Kim *et al.*[59] conducted research on the delivery of siRNA using mesoporous bioactive glass nanospheres and examined how it influenced osteoclastogenesis *in vitro*. Their results indicated significant inhibition of osteoclast formation *via* TRAP staining and the expression of osteoclastogenesis-related genes. Wang *et al.* also demonstrated that transfecting RAW264.7 and primary bone marrow cell cultures with RANK-specific siRNA resulted in significant inhibition of osteoclast formation and bone resorption.[60] In this study, we performed TRAP staining to evaluate osteoclast differentiation. TRAP is abundantly expressed by the osteoclast during bone resorption, which is considered as a marker for osteoclast formation.[61] As shown in Fig. 6(A), osteoclast precursors differentiated into multinucleated giant osteoclasts with $TRAP^+$ staining within 7 d in the presence of M-CSF and RANKL. However, treatment with bioactive MDs-NFATc1 resulted in a significant reduction in $TRAP^+$ osteoclasts (ESI,† Fig. S2). Additionally, the $TRAP^+$ osteoclasts in the MDs-scramble group showed no difference compared with the control. The critical role of NFATc1 in osteoclast differentiation and the expression of osteoclast-specific genes has been suggested previously.[26,62] For instance, Aliprantis *et al.* generated conditional NFATc1 knockout mice and found that the deletion of NFATc1 in young mice resulted in suppression of osteoclastogenesis and

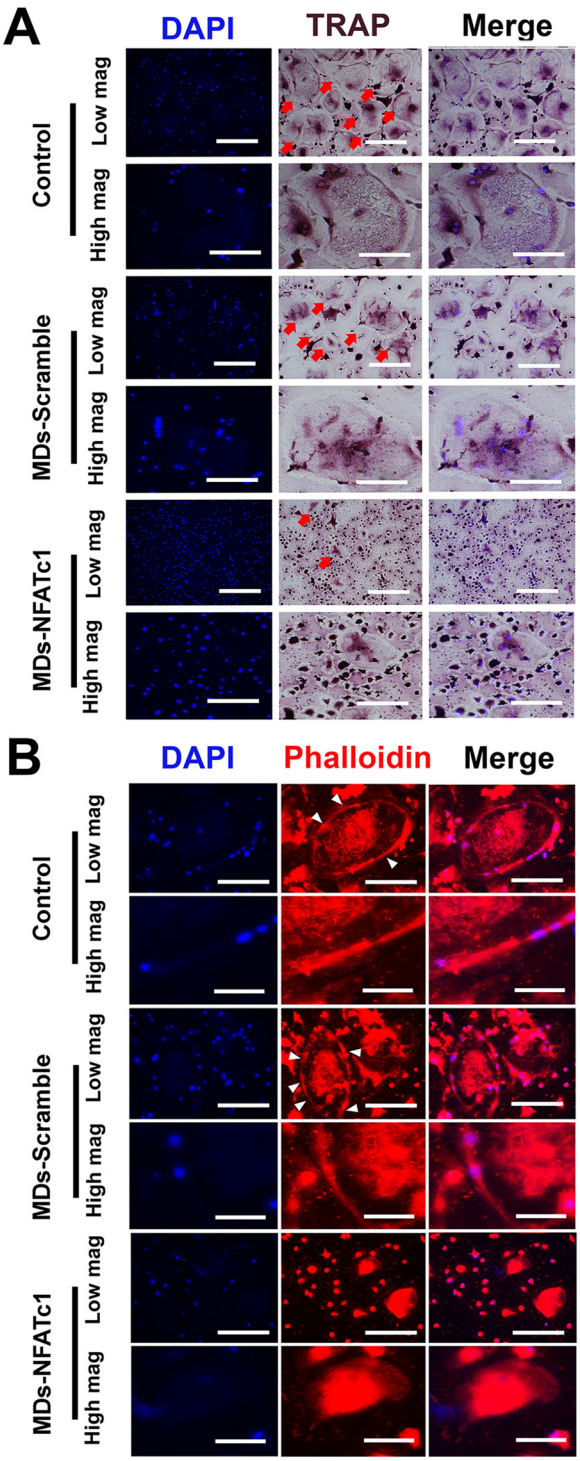

Fig. 6 Osteoclast differentiation and formation. (A) Representative TRAP staining images. The osteoclast precursor cells were cultured with an osteoclast precursor growth medium supplemented with different formulations of MDs for 7 days. Scale bar = 400 μm (low magnification). Scale bar = 250 μm (high magnification). The osteoclasts are denoted by the white arrow. (B) Representative confocal laser microscopy images of actin ring formation. Osteoclast precursor cells were seeded on 24-well coverslips and cultured with different formulations of MDs in the presence of RANKL and M-CSF for 7 days. Cells were fixed and examined by immunofluorescence after phalloidin and DAPI dual staining. Scale bar = 250 μm (low magnification). Scale bar = 50 μm (high magnification).

osteoclast-deficient osteopetrosis[62] *in vivo* and impaired osteoclast differentiation *in vitro*, which is consistent with our results.

To determine the effect of different formulations of MDs on actin ring formation in mature osteoclasts, immunofluorescence staining assay was performed. Osteoclast actin ring is an indispensable actin structure that is essential for osteoclast bone resorption.[63] As depicted in Fig. 6(B), the impact of MDs-NFATc1 on osteoclast formation was confirmed through immunofluorescence staining. The control and MDs-scramble groups exhibited large F-actin rings, whereas MDs-NFATc1 treatment notably reduced the sizes of the F-actin rings. Similarly, no significant difference was noted between control and MDs-scramble groups. We next evaluated the impact of MDs-NFATc1 on *in vitro* bone resorption. The results revealed notable inhibitory effects on osteoclast-mediated bone resorption following treatment with MDs-NFATc1 (ESI,† Fig. S3).

Bioactive MDs-NFATc1 prevents osteoporosis in OVX rats

After observing the inhibitory effects of MDs-NFATc1 on osteoclast differentiation and function *in vitro*, we next evaluated the potential restorative effects of MDs-NFATc1 in an *in vivo* model of bone loss induced by ovariectomy (OVX). The OVX model is commonly used to mimic postmenopausal osteoporosis, characterized by increased bone resorption and reduced bone formation.[64]

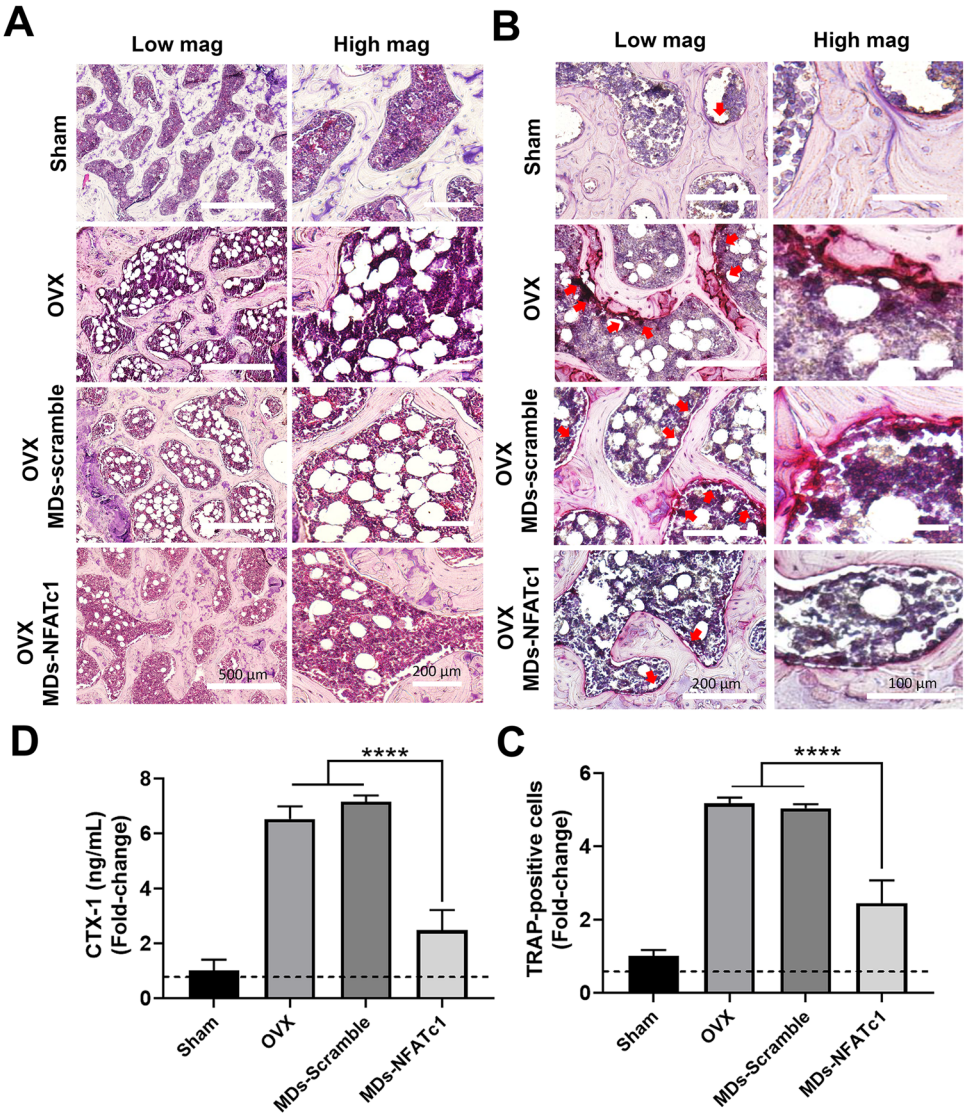

Fig. 7 The effects of MDs-NFATc1 on osteoporotic bone loss in OVX rats. (A) Representative H&E staining of femoral sections at 10 weeks post-treatment. The sections were stained using hematoxylin and eosin and were examined using an inverted microscope with a ×10 objective. In the OVX and OVX + MDs-scramble groups, a significant increase of adipocytes replacing the trabeculae and bone marrow was observed. However, following MDs-NFATc1 treatment, the presence of trabeculae along with a reduced number of adipocytes in the bone marrow was observed. (B) Representative TRAP-stained histologic sections from the sham, OVX, OVX + MDs-scramble, and OVX + MDs-NFATc1 groups are presented. TRAP staining was used to stain the osteoclasts, indicating osteoclast activity. (C) Quantification of TRAP-positive cells revealed a significant difference between OVX and OVX + MDs-NFATc1 groups (****$p < 0.0001$). (D) The serum levels of the bone resorption marker CTX-1 were analyzed using an ELISA. Treatment with MDs-NFATc1 resulted in a significant reduction in the level of CTX-1, indicating a decrease in bone resorption. ****$p < 0.0001$.

Numerous siRNA-guided delivery systems have emerged as potential therapies for osteoporosis. For instance, Cui and colleagues introduced an engineered exosome-based Shn3 siRNA delivery system designed for osteoporosis treatment. Their findings demonstrated an anti-osteoporotic effect in an OVX-induced bone loss model.[65] Natural miRNA cargos delivered by bioinspired nanovesicles have also shown efficacy for treating osteoporosis.[66] To explore the potential effects of MDs-NFATc1 on pathological bone loss induced by OVX, histological analysis of HE-stained sections was performed. As shown in Fig. 7(A), rats in the OVX group exhibited noticeable bone loss characterized by a higher accumulation of adipocytes in the bone marrow compared to the sham group. Accumulation of bone marrow adipose tissue is a common phenomenon observed in various conditions, including postmenopausal osteoporosis.[67] These fat reservoirs play significant regulatory roles within the skeletal system through the secretion of adipokines, inflammatory factors, and various other molecules.[68,69] However, rats treated with MDs-NFATc1 demonstrated significant resistance to OVX-induced bone loss. This was evident by the presence of a bony structure resembling that of the sham group and a reduction in adipocyte infiltration in the bone marrow. These findings indicate that MDs-NFATc1 treatment offers protective effects against the pathological changes induced by OVX in bone tissue.

To evaluate the effect of MDs-NFATc1 on osteoclastogenesis, TRAP staining was performed. As shown in Fig. 7(B) and (C), TRAP staining results revealed a significant increase in the number of TRAP-positive multinucleated giant cells in the OVX group. Following OVX, there is an upregulation of osteoclastogenesis, leading to an increased number and activity of osteoclasts.[70] This enhanced osteoclast differentiation and function contribute to the accelerated bone resorption observed in OVX-induced bone loss. In our study, the OVX + MDs-NFATc1 group exhibited a significant reduction in the number of osteoclasts. The absence of NFATc1 prevents proper osteoclast formation, resulting in impaired bone resorption and an accumulation of dense bone tissue as conditional knockout of NFATc1 resulted in inhibition of osteoclastogenesis both *in vitro* and *in vivo*.[62] These results indicate that MDs-NFATc1 treatment effectively suppresses osteoclast formation in the OVX animal model, indicating its potential role in regulating osteoclastogenesis and maintaining bone homeostasis.

To assess the effect of MDs-NFATc1 on serum levels of CTX-1, a marker of bone resorption, CTX-1, was quantified using CTX-1 ELISA assay. CTX-1 is a fragment released during the degradation of type I collagen, which is the major component of bone matrix.[71] CTX-1 is released into the bloodstream during the process of bone resorption by osteoclasts. As shown in Fig. 7(D), OVX animals showed an elevated serum CTX-1 level in comparison to the sham group. However, treatment with MDs-NFATc1 significantly reduced the serum CTX-1 level when compared to both the OVX and MDs-Scramble treated groups. These findings suggest that MDs-NFATc1 treatment effectively decreases bone resorption, as evidenced by the reduction in serum CTX-1 levels.

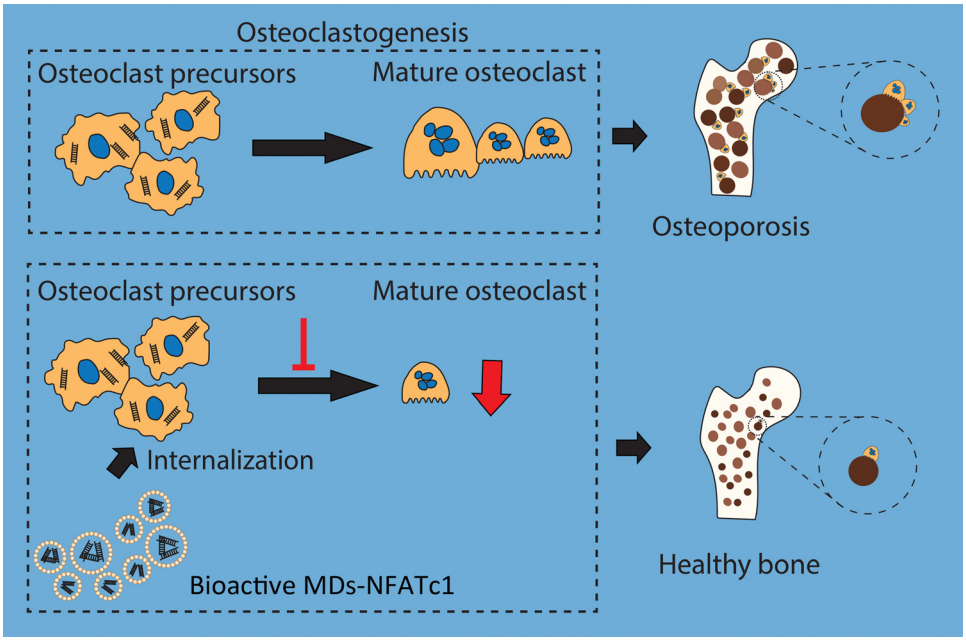

Fig. 8 Schematic diagram showing the bioactive MDs-NFATc1 targeting osteoclastogenesis. Osteoporosis is a skeletal disorder characterized by reduced bone strength and excessive osteoclast activities. Originating from the hemopoietic cells of the monocyte/macrophage lineage, activation of osteoclast-specific genes is essential for osteoclast formation. The RANKL/RANK interaction is crucial for the differentiation of osteoclast precursors to osteoclasts. The expression and translocation of NFATc1 is an essential regulator for osteoclast functions. Here, we report the fabrication of bioactive MDs targeting bone-resorbing osteoclast formation, which showed good biocompatibility and could be used as a novel anti-bone resorption therapy for osteoclast activation.

Conclusions

In conclusion, we fabricated bioactive MDs encapsulated with NFATc1-siRNA that specifically target osteoclast formation in order to reverse imbalanced osteoclast activation (Fig. 8). Imbalance between osteoclastogenesis and osteoblast-mediated bone formation has been considered as the main cause of many bone diseases. Our results indicated that these bioactive MDs showed no cytotoxicity in RAW 264.7 macrophages and hBMSCs. Our results further indicated that these bioactive MDs can significantly inhibit osteoclastogenesis and osteoclast differentiation. By utilizing the OVX-induced osteoporotic animal model, we evaluated the therapeutic potential of MDs-NFATc1 for postmenopausal osteoporosis. Treatment with MDs-NFATc1 in the rats demonstrated a significant protective effect against bone loss induced by OVX. The administration of MDs-NFATc1 effectively prevented or attenuated the deterioration of bone density and structure in the OVX model. These findings suggest that MDs-NFATc1 treatment holds promise for mitigating the detrimental effects of OVX-induced bone loss, preserving bone integrity and inhibiting excessive osteoclast activity. However, this study has several limitations. First, we exclusively assessed the efficacy of a single MDs-NFATc1 dose in preventing OVX development. In the future, it would be interesting to explore multiple doses, including low, medium, and high dosages, to comprehensively evaluate its effectiveness. Second, our study focused solely on a single and relatively late-stage time point for OVX assessment, which restricted our capability to fully evaluate the dynamics of bone loss. Therefore, an early/intermediate time point might be necessary for future investigations. Third, it is necessary to incorporate μCT data for a comprehensive assessment of the bone protective efficacy of MDs-NFATc1 in the future. Additionally, it is important to employ alternative methods, such as western blot or immunohistochemistry, to assess the expression of markers associated with osteoclasts *in vitro* and *in vivo*. Lastly, for a more comprehensive study, it would be necessary to include estrogen as a positive control since OVX is an established model for bone loss attributed to estrogen deficiency.

Author contributions

All authors made substantial contributions to conception and design, acquisition of the data, or analysis and interpretation of the data; took part in drafting the article or revising it critically for important intellectual content; gave final approval of the version to be published; and agreed to be accountable for all aspects of the work.

Conflicts of interest

The authors declare that they have no competing interests.

Acknowledgements

This work was financially supported by the National Natural Science Foundation of China (grant no. 82060620, 31960209, and 82260440), the Outstanding Youth Scientific Fund of Guizhou Province (grant no. Qian Ke He Platform Talents YQK[2023] 039), the Guizhou Science and Technology Fund Project (grant no. [2020]1Y093), the Guizhou Science and Technology Program Project (grant no. Qiankehe Foundation – ZK[2023] General 502), the Science and Technology Fund Project of Guizhou Provincial Health Commission (grant no. gzwkj 2022-108), the Guizhou Province Colleges and Universities Youth Science and Technology Talent development project (grant no. Qian Jiao He KY Zi 283 [2022]), the Zunyi Science and Technology Fund Project (grant no. Zunyi Kehe HZ Zi [2021]40), the Future Eminent Clinician Plan of Zunyi Medical University (grant no. 2022-02), and Affiliated Hospital of Zunyi Medical University Doctoral Research Start-up Fund Project (grant no. 2022-5).

References

1 N. E. Lane, Epidemiology, etiology, and diagnosis of osteoporosis, *Am. J. Obstet. Gynecol.*, 2006, **194**(2 Suppl.), S3–S11.
2 Y. Guo, Y. Liu, C. Shi, T. Wu, Y. Cui, S. Wang, P. Liu, X. Feng, Y. He and D. Fu, Remote-controllable bone-targeted delivery of estradiol for the treatment of ovariectomy-induced osteoporosis in rats, *J. Nanobiotechnol.*, 2021, **19**(1), 248.
3 S. W. Blume and J. R. Curtis, Medical costs of osteoporosis in the elderly Medicare population, *Osteoporosis Int.*, 2011, **22**(6), 1835–1844.
4 N. Harvey, E. Dennison and C. Cooper, Osteoporosis: impact on health and economics, *Nat. Rev. Rheumatol.*, 2010, **6**(2), 99–105.
5 M. A. Clynes, N. C. Harvey, E. M. Curtis, N. R. Fuggle, E. M. Dennison and C. Cooper, The epidemiology of osteoporosis, *Br. Med. Bull.*, 2020, **133**(1), 105–117.
6 S. R. Cummings and L. J. Melton, Epidemiology and outcomes of osteoporotic fractures, *Lancet*, 2002, **359**(9319), 1761–1767.
7 L. Xiao, Y. Ma, R. Crawford, J. Mendhi, Y. Zhang, H. Lu, Q. Zhao, J. Cao, C. Wu and X. Wang, The interplay between hemostasis and immune response in biomaterial development for osteogenesis, *Mater. Today*, 2022, **54**, 202–224.
8 J. Y. Noh and Y. Yang, Molecular mechanisms and emerging therapeutics for osteoporosis, *Int. J. Mol. Sci.*, 2020, **21**(20), 7623.
9 R. A. Adler, G. El-Hajj Fuleihan, D. C. Bauer, P. M. Camacho, B. L. Clarke, G. A. Clines, J. E. Compston, M. T. Drake, B. J. Edwards, M. J. Favus, S. L. Greenspan, R. McKinney, Jr., R. J. Pignolo and D. E. Sellmeyer, Managing osteoporosis in patients on long-term bisphosphonate treatment: Report of a task force of the american society for bone and mineral research, *J. Bone Miner. Res.*, 2016, **31**(1), 16–35.
10 T. Ponnapakkam, R. Katikaneni, J. Sakon, R. Stratford and R. C. Gensure, Treating osteoporosis by targeting parathyroid hormone to bone, *Drug Discovery Today*, 2014, **19**(3), 204–208.

11 J. Li, A. Xi, H. Qiao and Z. Liu, Ultrasound-mediated diagnostic imaging and advanced treatment with multifunctional micro/nanobubbles, *Cancer Lett.*, 2020, **475**, 92–98.
12 H. Wu, E. C. Abenojar, R. Perera, A. C. De Leon, T. An and A. A. Exner, Time-intensity-curve analysis and tumor extravasation of nanobubble ultrasound contrast agents, *Ultrasound Med. Biol.*, 2019, **45**(9), 2502–2514.
13 P. Nittayacharn, H. X. Yuan, C. Hernandez, P. Bielecki, H. Zhou and A. A. Exner, Enhancing tumor drug distribution with ultrasound-triggered nanobubbles, *J. Pharm. Sci.*, 2019, **108**(9), 3091–3098.
14 C. Su, X. Ren and F. Nie, Current advances in ultrasound-combined nanobubbles for cancer-targeted therapy: a review of the current status and future perspectives, *RSC Adv.*, 2021, **11**(21), 12915–12928.
15 B. H. Tan, H. An and C. D. Ohl, How bulk nanobubbles might survive, *Phys. Rev. Lett.*, 2020, **124**(13), 134503.
16 R. Cavalli, A. Bisazza, M. Trotta, M. Argenziano, A. Civra, M. Donalisio and D. Lembo, New chitosan nanobubbles for ultrasound-mediated gene delivery: preparation and *in vitro* characterization, *Int. J. Nanomed.*, 2012, **7**, 3309–3318.
17 E. E. Marxer, J. Brüssler, A. Becker, J. Schümmelfeder, R. Schubert, C. Nimsky and U. Bakowsky, Development and characterization of new nanoscaled ultrasound active lipid dispersions as contrast agents, *Eur. J. Pharm. Biopharm.*, 2011, **77**(3), 430–437.
18 B. E. O'Neill and N. Rapoport, Phase-shift, stimuli-responsive drug carriers for targeted delivery, *Ther. Delivery*, 2011, **2**(9), 1165–1187.
19 X. Cai, Y. Jiang, M. Lin, J. Zhang, H. Guo, F. Yang, W. Leung and C. Xu, Ultrasound-responsive materials for drug/gene delivery, *Front. Pharmacol.*, 2019, **10**, 1650.
20 A. L. Klibanov, T. I. Shevchenko, B. I. Raju, R. Seip and C. T. Chin, Ultrasound-triggered release of materials entrapped in microbubble-liposome constructs: a tool for targeted drug delivery, *J. Controlled Release*, 2010, **148**(1), 13–17.
21 C. Yan, D. Zhu, D. Huang and G. Xia, Role of ultrasound and microbubble-mediated heat shock protein 72 siRNA on ischemia-reperfusion liver injury in rat, *Int. J. Clin. Exp. Med.*, 2015, **8**(4), 5746–5752.
22 J. A. Alvarez-Fernández, Ultrasound-enhanced systemic thrombolysis. An effective and underutilized treatment for acute ischemic stroke, *Med. Intensiva*, 2011, **35**(2), 134–135.
23 C. Y. Lin, H. Y. Hsieh, C. M. Chen, S. R. Wu, C. H. Tsai, C. Y. Huang, M. Y. Hua, K. C. Wei, C. K. Yeh and H. L. Liu, Non-invasive, neuron-specific gene therapy by focused ultrasound-induced blood-brain barrier opening in Parkinson's disease mouse model, *J. Controlled Release*, 2016, **235**, 72–81.
24 R. Huang, X. Wang, Y. Zhou and Y. Xiao, RANKL-induced M1 macrophages are involved in bone formation, *Bone Res.*, 2017, **5**, 17019.
25 Y. Dong, K. Song, P. Wang, J. Guo, H. Kang, X. Tan, B. Zhu, R. Peng, M. Zhu, K. Yu, Q. Guo, H. Guan and F. Li, Blocking the cytohesin-2/ARF1 axis by SecinH3 ameliorates osteoclast-induced bone loss *via* attenuating JNK-mediated IRE1 endoribonuclease activity, *Pharmacol. Res.*, 2022, **185**, 106513.
26 J. H. Kim and N. Kim, Regulation of NFATc1 in osteoclast differentiation, *J. Bone Metab.*, 2014, **21**(4), 233–241.
27 J. H. Park, N. K. Lee and S. Y. Lee, Current understanding of RANK signaling in osteoclast differentiation and maturation, *Mol. Cells*, 2017, **40**(10), 706–713.
28 Y. Zhang, J. Cao, M. Jian, Z. Zhou, N. Anwar, L. Xiao, Y. Ma, D. Zhang, J. Zhang and X. Wang, Fabrication of Interleukin-4 Encapsulated Bioactive Microdroplets for Regulating Inflammation and Promoting Osteogenesis, *Int. J. Nanomed.*, 2023, **18**, 2019–2035.
29 F. Wei, G. Liu, Y. Guo, R. Crawford, Z. Chen and Y. Xiao, Blood prefabricated hydroxyapatite/tricalcium phosphate induces ectopic vascularized bone formation *via* modulating the osteoimmune environment, *Biomater. Sci.*, 2018, **6**(8), 2156–2171.
30 A. Tasset and A. Bellamkonda, Overcoming barriers in non-viral gene delivery for neurological applications, *Nanoscale*, 2022, **14**(10), 3698–3719.
31 J. Wang, Z. Lu, M. G. Wientjes and J. L. Au, Delivery of siRNA therapeutics: barriers and carriers, *AAPS J.*, 2010, **12**(4), 492–503.
32 M. I. Sajid and M. Moazzam, Overcoming barriers for siRNA therapeutics: From bench to bedside, *Pharmaceuticals*, 2020, **13**(10), 294.
33 B. Hu, L. Zhong, Y. Weng, L. Peng and Y. Huang, Therapeutic siRNA: State of the art, *Signal Transduction Targeted Ther.*, 2020, **5**(1), 101.
34 N. C. Smith, M. L. Rise and S. L. Christian, A comparison of the innate and adaptive immune systems in cartilaginous fish, ray-finned fish, and lobe-finned fish, *Front. Immunol.*, 2019, **10**, 2292.
35 D. H. Yang and M. Y. Yang, The role of macrophage in the pathogenesis of osteoporosis, *Int. J. Mol. Sci.*, 2019, **20**(9), 2093.
36 C. F. Anderson and D. M. Mosser, A novel phenotype for an activated macrophage: the type 2 activated macrophage, *J. Leukocyte Biol.*, 2002, **72**(1), 101–106.
37 L. Ginaldi, M. C. Di Benedetto and M. De Martinis, Osteoporosis, inflammation and ageing, *Immun. Ageing*, 2005, **2**, 14.
38 J. Muñoz, N. S. Akhavan, A. P. Mullins and B. H. Arjmandi, Macrophage polarization and osteoporosis: A review, *Nutrients*, 2020, **12**(10), 2999.
39 K. Chen, Y. Jiao, L. Liu, M. Huang, C. He, W. He, J. Hou, M. Yang, X. Luo and C. Li, Communications between bone marrow macrophages and bone cells in bone remodeling, *Front. Cell Dev. Biol.*, 2020, **8**, 598263.
40 O. Tysoe, Osteal macrophages implicated in osteoporosis, *Nat. Rev. Endocrinol.*, 2021, **17**(10), 577.
41 C. Atri and F. Z. Guerfali, Role of human macrophage polarization in inflammation during infectious diseases, *Int. J. Mol. Sci.*, 2018, **19**(6), 1801.
42 T. Rőszer, Understanding the mysterious M2 macrophage through activation markers and effector mechanisms, *Mediators Inflammation*, 2015, **2015**, 816460.

43 V. Nagy and M. Watzele, FuGENE® 6 transfection reagent: minimizing reagent-dependent side effects as analyzed by gene-expression profiling and cytotoxicity assays, *Nat. Methods*, 2006, **3**(5), iii–v.
44 T. Wang, L. M. Larcher, L. Ma and R. N. Veedu, Systematic screening of commonly used commercial transfection reagents towards efficient transfection of single-stranded oligonucleotides, *Molecules*, 2018, **23**(10), 2564.
45 M. Ghasemi, T. Turnbull, S. Sebastian and I. Kempson, The MTT assay: Utility, limitations, pitfalls, and interpretation in bulk and single-cell analysis, *Int. J. Mol. Sci.*, 2021, **22**(23), 12827.
46 X. Chen, Y. Li, R. He and Q. Ding, Phenotyping field-state wheat root system architecture for root foraging traits in response to environment × management interactions, *Sci. Rep.*, 2018, **8**(1), 2642.
47 N. Ma, M. K. Zhang, X. S. Wang, L. Zhang, J. Feng and X. Z. Zhang, NIR light-triggered degradable $MoTe_2$ nanosheets for combined photothermal and chemotherapy of cancer, *Adv. Funct. Mater.*, 2018, **28**(31), 1801139.
48 I. R. Murray and B. Péault, Q&A: Mesenchymal stem cells – where do they come from and is it important?, *BMC Biol.*, 2015, **13**, 99.
49 A. Musiał-Wysocka, M. Kot and M. Majka, The pros and cons of mesenchymal stem cell-based therapies, *Cell Transplant.*, 2019, **28**(7), 801–812.
50 H. Kim, C. Bae, Y. M. Kook, W. G. Koh, K. Lee and M. H. Park, Mesenchymal stem cell 3D encapsulation technologies for biomimetic microenvironment in tissue regeneration, *Stem Cell Res. Ther.*, 2019, **10**(1), 51.
51 R. Berebichez-Fridman and P. R. Montero-Olvera, Sources and clinical applications of mesenchymal stem cells: State-of-the-art review, *Sultan Qaboos Univ. Med. J.*, 2018, **18**(3), e264–e277.
52 C. W. Park, K. S. Kim, S. Bae, H. K. Son, P. K. Myung, H. J. Hong and H. Kim, Cytokine secretion profiling of human mesenchymal stem cells by antibody array, *Int. J. Stem Cells*, 2009, **2**(1), 59–68.
53 A. A. Al-Bari and A. Al Mamun, Current advances in regulation of bone homeostasis, *FASEB BioAdv.*, 2020, **2**(11), 668–679.
54 J. S. Brunner, L. Vulliard, M. Hofmann, M. Kieler, A. Lercher, A. Vogel, M. Russier, J. B. Brüggenthies, M. Kerndl and V. Saferding, Environmental arginine controls multinuclear giant cell metabolism and formation, *Nat. Commun.*, 2020, **11**(1), 1–15.
55 B. F. Boyce, Z. Yao and L. Xing, Osteoclasts have multiple roles in bone in addition to bone resorption, *Crit. Rev. Eukaryotic Gene Expression*, 2009, **19**(3), 171–180.
56 J. Yang, R. Tang, J. Yi, Y. Chen, X. Li, T. Yu and J. Fei, Diallyl disulfide alleviates inflammatory osteolysis by suppressing osteoclastogenesis *via* NF-κB-NFATc1 signal pathway, *FASEB J.*, 2019, **33**(6), 7261–7273.
57 N. K. Lee, RANK signaling pathways and key molecules inducing osteoclast differentiation, *Biomed. Sci. Lett.*, 2017, **23**(4), 295–302.
58 N. A. Hamdy, Denosumab: RANKL inhibition in the management of bone loss, *Drugs Today*, 2008, **44**(1), 7–21.
59 T. H. Kim, R. K. Singh, M. S. Kang, J. H. Kim and H. W. Kim, Inhibition of osteoclastogenesis through siRNA delivery with tunable mesoporous bioactive nanocarriers, *Acta Biomater.*, 2016, **29**, 352–364.
60 Y. Wang and D. W. Grainger, siRNA knock-down of RANK signaling to control osteoclast-mediated bone resorption, *Pharm. Res.*, 2010, **27**(7), 1273–1284.
61 K. Harada, H. Itoh, Y. Kawazoe, S. Miyazaki, K. Doi, T. Kubo, Y. Akagawa and T. Shiba, Polyphosphate-mediated inhibition of tartrate-resistant acid phosphatase and suppression of bone resorption of osteoclasts, *PLoS One*, 2013, **8**(11), e78612.
62 A. O. Aliprantis, Y. Ueki, R. Sulyanto, A. Park, K. S. Sigrist, S. M. Sharma, M. C. Ostrowski, B. R. Olsen and L. H. Glimcher, NFATc1 in mice represses osteoprotegerin during osteoclastogenesis and dissociates systemic osteopenia from inflammation in cherubism, *J. Clin. Invest.*, 2008, **118**(11), 3775–3789.
63 T. Matsubara, M. Kinbara, T. Maeda, M. Yoshizawa, S. Kokabu and T. Takano Yamamoto, Regulation of osteoclast differentiation and actin ring formation by the cytolinker protein plectin, *Biochem. Biophys. Res. Commun.*, 2017, **489**(4), 472–476.
64 N. Yousefzadeh, K. Kashfi, S. Jeddi and A. Ghasemi, Ovariectomized rat model of osteoporosis: a practical guide, *EXCLI J.*, 2020, **19**, 89–107.
65 Y. Cui, Y. Guo, L. Kong, J. Shi, P. Liu, R. Li, Y. Geng, W. Gao, Z. Zhang and D. Fu, A bone-targeted engineered exosome platform delivering siRNA to treat osteoporosis, *Bioact. Mater.*, 2022, **10**, 207–221.
66 Y. Cui, Z. Li, Y. Guo, X. Qi, Y. Yang, X. Jia, R. Li, J. Shi, W. Gao, Z. Ren, G. Liu, Q. Ye, Z. Zhang and D. Fu, Bioinspired Nanovesicles Convert the Skeletal Endothelium-Associated Secretory Phenotype to Treat Osteoporosis, *ACS Nano*, 2022, **16**(7), 11076–11091.
67 N. Aaron, S. Costa, C. J. Rosen and L. Qiang, The Implications of Bone Marrow Adipose Tissue on Inflammaging, *Front. Endocrinol.*, 2022, **13**, 853765.
68 M. Okla and M. Kassem, Thermogenic potentials of bone marrow adipocytes, *Bone*, 2021, **143**, 115658.
69 Y. Li, Y. Meng and X. Yu, The Unique Metabolic Characteristics of Bone Marrow Adipose Tissue, *Front. Endocrinol.*, 2019, **10**, 69.
70 J. Y. Li, H. Tawfeek, B. Bedi, X. Yang, J. Adams, K. Y. Gao, M. Zayzafoon, M. N. Weitzmann and R. Pacifici, Ovariectomy disregulates osteoblast and osteoclast formation through the T-cell receptor CD40 ligand, *Proc. Natl. Acad. Sci. U. S. A.*, 2011, **108**(2), 768–773.
71 S. A. Chubb, Measurement of C-terminal telopeptide of type I collagen (CTX) in serum, *Clin. Biochem.*, 2012, **45**(12), 928–935.

